Simulations towards the achievement of non-inductive current ramp-up and sustainment in the National Spherical Torus Experiment Upgrade

2015 Nucl. Fusion 55 123011

(http://iopscience.iop.org/0029-5515/55/12/123011)

IOP Publishing | International Atomic Energy Agency Nuclear Fusion

Nucl. Fusion **55** (2015) 123011 (12pp) doi:10.1088/0029-5515/55/12/123011

Simulations towards the achievement of non-inductive current ramp-up and sustainment in the National Spherical Torus Experiment Upgrade

F.M. Poli, R.G. Andre, N. Bertelli, S.P. Gerhardt, D. Mueller and G. Taylor

Princeton Plasma Physics Laboratory, Princeton, NJ 08543, USA

E-mail: fpoli@pppl.gov

Received 17 March 2015, revised 10 September 2015
Accepted for publication 7 October 2015
Published 30 October 2015

Abstract

One of the goals of the National Spherical Torus Experiment Upgrade (NSTX-U) (Menard *et al* 2012 *Nucl. Fusion* **52** 083015) is the demonstration of fully non-inductive start-up, current ramp-up and sustainment. This work discusses predictive simulations where the available heating and current drive systems are combined to maximize the non-inductive current and minimize the solenoidal contribution. Radio-frequency waves at harmonics higher than the ion cyclotron resonance (high-harmonic fast waves (HHFW)) and neutral beam injection are used to ramp the plasma current non-inductively starting from an initial Ohmic plasma.

An interesting synergy is observed in the simulations between the HHFW and electron cyclotron (EC) wave heating. Time-dependent simulations indicate that, depending on the phasing of the HHFW antenna, EC wave heating can significantly increase the effectiveness of the radio-frequency power, by heating the electrons and increasing the current drive efficiency, thus relaxing the requirements on the level of HHFW power that needs to be absorbed in the core plasma to drive the same amount of fast-wave current.

Keywords: ramp-up, non-inductive, magnetic fusion, neutral beams, radio frequency waves

(Some figures may appear in colour only in the online journal)

1. Introduction

The Spherical Torus (ST) [1, 2] is a leading candidate for a fusion nuclear science facility (FNSF) due to its compact size and modular configuration [3, 4]. The high neutron wall load, the high values of β (plasma pressure to magnetic pressure ratio) achievable and the ease of maintenance make the ST an attractive option for nuclear component test facilities [5].

Critical elements of ST research in support of steady-state operation and demonstration of the viability of the ST as a fusion power plant include sustainment of fully non-inductive current with large bootstrap current fraction [5, 6], non solenoidal start-up and ramp-up [5] and operation at high β and high confinement with resistive wall mode stabilization [7].

The start-up, ramp-up, and sustainment of a tokamak plasma utilizing little to no induction from a central solenoid is a major challenge in magnetic fusion. In particular, the development of techniques to minimize or eliminate the central solenoid is critical to the design of compact electricity-producing fusion power plants based on the ST concept and could also benefit advanced tokamak reactors. Eliminating the central solenoid would simplify engineering design and reduce costs.

The issue of non-inductive start-up of conventional and spherical tokamaks has long history, for example using LH [8–10] and RF in the range of frequency of EC/EBW [11–20]. The method of coaxial helicity injection (CHI) relies on electrostatic helicity injection for initiating the plasma discharge [21]. Transient CHI has successfully demonstrated the

formation of high-quality closed flux plasma in NSTX with a flux saving with respect to ohmic start-up [22–24] and will be used as a front end of the start-up method for a full demonstration of non-inductive current start-up [24, 25]. Simulations project CHI to be capable of generating over 400–600 kA of closed flux surfaces in NSTX-U, operating at full toroidal field [5, 25].

Future ST-FNSF are projected to rely on neutral beam injection (NBI) to sustain about 50% of the plasma current, with the remainder provided by the self-generated bootstrap current. In addition, NBI is also envisioned to provide heating and current drive for non-inductive current ramp-up. In order to assess non-inductive advanced scenarios for ST-FNSF, the National Spherical Torus eXperiment (NSTX) [26, 27] is undergoing a major upgrade (NSTX-U) [5] to double the toroidal field from 0.55 T and 1 s duration to 1 T and 6 s duration. The size of the ohmic solenoid has been tripled to provide the flux required to extend the range of inductively driven plasmas that can be studied on NSTX-U up to 2 MA of plasma current for 5 s at full magnetic field.

Extensive simulations have been previously undertaken to define the equilibrium operating space in NSTX-U [6]. Scenarios were defined over fully relaxed equilibria, extrapolating from experimental NSTX density and temperature profiles. Thermal pressure peaking, Greenwald density fraction, thermal ion transport and outer gap were identified as critical elements in determining the operational space. This work discusses time-dependent simulations of current ramp-up and sustainment with NBI and Radio Frequency (RF) waves, and discusses some of the issues that require validation and that need to be addressed in experiments. The simulations, run with free-boundary TRANSP [28, 29], evolve self-consistently the equilibrium, the heating and current drive sources and the pressure profiles, within the limits of the physics model used to predict energy transport. Self-consistent evolution is particularly important in the non-inductive ramp-up. Pressure and externally driven current profiles undergo variations over short time scales and may exhibit large spatial gradients. The equilibrium and the kinetic profiles must be evolved self-consistently, while ensuring at the same time adequate control of the plasma position and shape. Time-dependent simulations of fully non-inductive startup and ramp-up to sustained flattop were previously done for NSTX for projection to NSTX-U [24] using the Tokamak Simulation Code TSC [30]. Although the code was modified to allow simulation of the CHI start-up, the discharge did not evolve the heating and current drive sources self-consistently with the kinetic profiles after start-up. Analytic heating profiles were used for the EC, HHFW and NBI and the temperature was evolved using a semi-empirical thermal transport model [31]. These simulations, which did not use direct RF current in the ramp-up and did not account for NBI losses, were therefore unable to identify all problems associated with modifications of the equilibrium in response to non-inductive current.

A description of the Heating and Current Drive sources and of the modeling tools is given in section 2. Section 3 discusses transport assumptions in the simulations. Section 4 discusses a simulation scenario where the two beamlines are used in combination with RF waves to ramp-up the current non-inductively to 0.7 MA and to sustain in the flattop for about 2 s. Section 5 discusses issues with using individual sources at start-up. Section 6 shows how using electron cyclotron (EC) waves for heating the start-up plasma would improve the absorption of RF waves and close the gap between the CHI start-up and the current ramp-up with high-harmonic fast waves (HHFW) and NBI. Finally, conclusions and future plans for experiments and validation are addressed in section 7.

2. Heating and current drive systems and calculations

2.1. Neutral beam injection

A second NBI system will add three sources to the existing, small tangency radius NBI system on NSTX, doubling the external heating and current drive capabilities. The second beamline, with larger tangency radii of 110, 120, 130 cm respectively, is designed to provide 100% non-inductive current for discharges with up to 1.3 MA [5].

Figure 1 shows the NBI system layout and summarizes the power and beam pulse duration as a function of the source voltage. Due to thermal limits of the ion dumps, the available pulse length on each beamline is reduced from 5 s to about 1.0 s as the beam energy and the total power available are increased from 3.3 MW (three sources with 65 kV) to 9 MW (three sources with 110 kV) [5]. Compared to the small tangency radius NBI system, the larger tangency radius is projected to increase the current drive efficiency by 40%, opening opportunities for control of current profiles and $q_{\min}$, for accessibility to high performance plasmas [6]. The NBI source model is the NUBEAM orbit following Monte Carlo code [32, 33], with current drive calculations that include collisionality dependence on shielding factor at arbitrary aspect ratio [34].

2.2. High harmonic fast waves

Fast waves at high harmonics of the ion cyclotron frequency are launched on NSTX-U at a frequency of 30 MHz with a large 12 strap antenna array that spans 90 degrees toroidally around the outside of the torus [35]. Spectra corresponding to parallel wavevectors of 3, 8, 13 m^{-1} can be selected by feeding the antenna with six decoupled sources [36]. The doubling of the magnetic field, while retaining the 30 MHz RF source frequency, moves the heating regime from the high harmonic used in NSTX to a mid harmonic fast wave regime. In particular, for deuterium majority ion and 0.55 T in NSTX the harmonic resonances inside the last close flux surface range from the 2nd/3rd to the 11th whereas, for 1 T, the harmonic resonances inside the last close flux surface range from the 2nd to the 5th [37]. The HHFW system is used in the simulation scenarios discussed herein to heat the start-up plasma, to assist with the L-H transition and to sustain up to 400 kA of non-inductive current during the time window where the NB cannot effectively drive current, because of large shine-thru at low density.

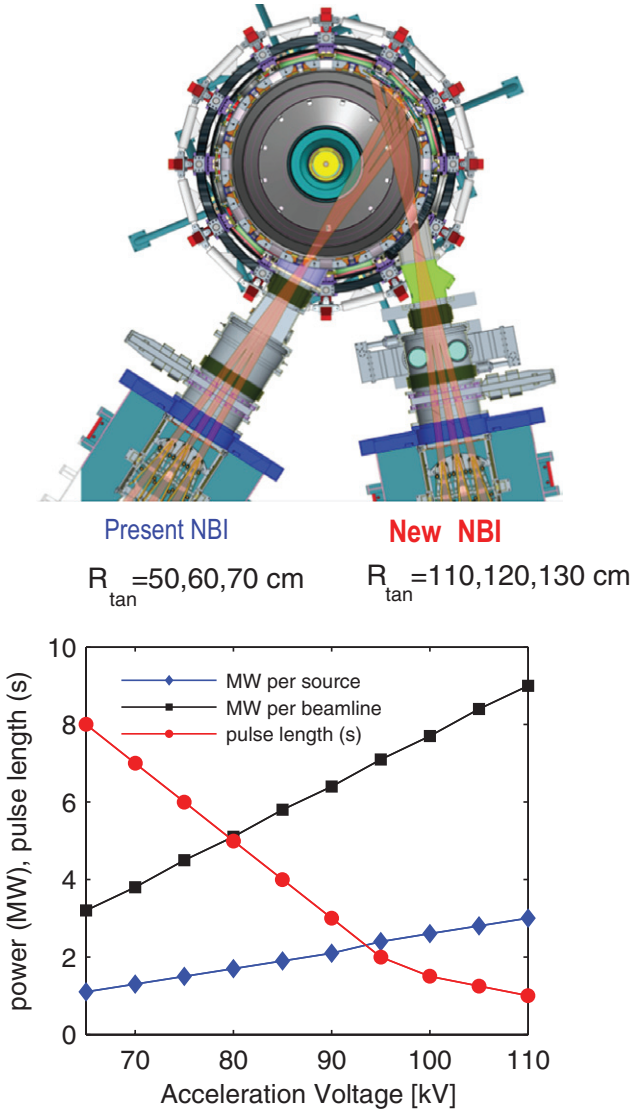

Figure 1. Left: layout of the beamlines. The first NBI has three sources at tangency radius of 50, 60, 70 cm; the second NBI has also three sources, aimed more tangential at 110, 120, 130 cm. Right: power per source (diamonds), power per beamline (squares) and pulse length (circles) for each value of source voltage.

The ICRF source model is the TORIC full wave [38] with an equivalent Maxwellian treatment for the fast ion species. The method to compute the FWCD in TORIC is based on Ehst-Karney parametrization [39], which provides a well-established formula for the RF current drive efficiency (including trapping particles) obtained starting from the adjoint method for the solution of the Fokker–Planck quasi-linear equation. The effective temperature of beam ions is calculated as $2E/3n_{\rm fast}$, where the fast ion density $n_{\rm fast}$ is calculated by NUBEAM and E is the average energy of the fast ion distribution, assuming a Maxwellian distribution.

2.3. Electron cyclotron waves heating

Electron cyclotron waves heat the plasma at the electron cyclotron resonance, which is given by $f\,[\mathrm{GHz}] = 28B_{\rm T}\,[\mathrm{T}]$. At this frequency, the waves are injected with O-mode polarization (with the wave electric field parallel to the magnetic field). With this polarization, the EC waves have a cut-off frequency at the electron plasma frequency $\omega_{pe} = (4\pi\ n_e e^2/m_e)^{0.5}$, where e, m_e n_e are the electron charge, mass and density respectively.

A megawatt-level 28 GHz electron cyclotron heating system is currently planned as an upgrade in NSTX-U in 2017–18 [40, 41]. The gyrotron can deliver up to 1 MW of power to the plasma over a pulse length of 1–5 s, which will be transmitted via a low-loss, corrugated $\mathrm{HE}_{1,\,1}$ waveguide [40, 41].

On NSTX-U and for 1 T magnetic field and a frequency of 28 GHz, the EC waves have a cutoff for the O-mode at a density of $9.72 \times 10^{18}\ \mathrm{m}^{-3}$. This limits the application of EC heating in NSTX-U to the early ramp-up phase.

The orientation of the mirror is fixed, pointing 5 degrees down and 1 degree right of the normal of the ECRH port. This is the position that maximizes first pass absorption, as it has been demonstrated by previous ray-tracing calculations over a typical CHI plasma target [40]. This steering injection configuration maximizes the electron heating, with minimum current drive.

The electron cyclotron heating and current drive are calculated with the GENRAY toroidal ray tracing code [42, 43], which includes an adjoint calculation of the electron cyclotron current drive efficiency that takes into account relativistic effects, trapped particle effects and momentum conserving corrections to the background collision operator [44, 45].

3. Transport assumptions

Predictive simulations depend on the thermal transport model used. Assessment of transport in H-mode will be undertaken in NSTX-U, including the pedestal structure, the L-H transition threshold and characterization of the NBI deposition, heating and current drive. In the absence of validation against NSTX-U like conditions, the simulations discussed herein are based on the results from transport models applied in NSTX plasma conditions.

A number of NSTX discharges have therefore been selected to assess thermal transport predictions. The selected cases include (a) a plasma with 300 kA current and 1.5 MW of HHFW that achieves fully non-inductive current drive operating at low density that is required to maximize the current drive efficiency (#138506) [46], (b) a 300 kA discharge with 1.5 MW of NBI (#140353), run for comparison with the RF discharge and (c) a 900 kA discharge with 200 ms ramp-up and NBI from the ramp-up phase (#142305) [47]. The latter will be also used as a reference for projections to non-inductive current ramp-up and sustainment in NSTX-U.

However, it should be noted that these reference cases, where the external sources are used in the flattop phase, do not describe the transient conditions of the plasma that is simulated here, where HHFW is used to ramp the current after start-up to values of 300–400 kA and where NBI is used afterwards for ramp-up to full current and sustainment. Experiments on NSTX-U with HHFW injection on low density, low temperature start-up plasmas, and NBI with current

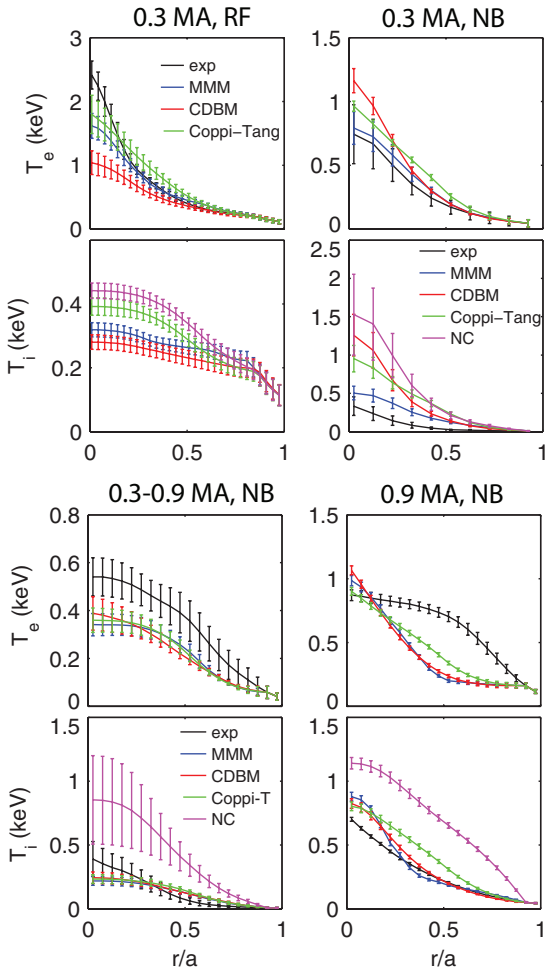

Figure 2. Comparison between the measured (black) temperature and the temperature predicted under different assumptions of the thermal transport, for NSTX discharges with RF and with NBI. Top panel: 300 kA L-mode flattop plasma with RF (left) and with NB (right). Bottom panel: 900 kA discharge with 5 MW of NBI, average profiles in the rampup (left) and in the flattop (right).

drive in excess of 400 kA will be necessary for a validation of the transport in this phase and for self-consistent projections from NSTX-U experiments to fully non-inductive start-up and current ramp-up in FNSF.

Figure 2 shows a comparison between the measured temperature and the temperature predicted under different assumptions on the thermal transport. Simulations have been run first with TRANSP in interpretative mode, then in predictive mode using various transport models: the MultiMode MMM7.1 [48], Coppi-Tang [49], the current diffusive ballooning mode model (CDBM) with plasma shape corrections [50] for both the ion and electron channel and neoclassical transport for the ion thermal transport, using the NCLASS NTCC libraries [51]. The profiles shown in figure 2 have been averaged over the heating phase both in the flattop cases and in the ramp-up heated phase with NBI. The error bars indicate the standard deviation from the average value during the heated phase.

In flattop discharges with 300 kA (top panel in figure 2), no model is systematically over- or under-predicting the electron or the ion temperature, with the CDBM giving the lowest average temperature in the RF heated discharge and the highest average value in the NBI heated discharge. The MMM7.1 model can reproduce the peaked profiles better than other models and in the NBI heated discharge at low current gives the closest agreement with the experiments. Ion temperature measurements are not available in the RF-only discharges, thus no conclusion can be drawn here on what model better reproduces the experiments. It should be noted that these plasmas are in L-mode.

In the discharge with NBI at 900 kA (bottom panel in figure 2), the models agree with each other, but none of them reproduce the broad electron temperature profile in the flattop. Good agreement among the turbulence models is also found in the ion temperature predictions, all in better agreement with experiments than the Neoclassical model, which tends to over-predict the ion temperature in all cases. In the ramp-up phase of the large current, NBI heated discharge (bottom panel, left column), the turbulence models are in good agreement to each other, within the standard deviation of profile variations in the time window considered. They can reproduce the profile peaking of the electron temperature profile, but all underestimate its amplitude. The measured ion temperature profile is more peaked than the predicted one, with differences outside error bars, the latter being significantly larger in this phase than in the flattop.

Based on this comparison, the MMM7.1 model is chosen for prediction of thermal electron and ion transport in the early ramp-up phase, up to 400 kA, where RF will be primarily used, either alone or in combination with NBI. During the NBI phase, where the current is ramped-up to 900 kA over a time window that spans between 2.5 and 5 s, experimental-like, analytic temperature profiles are used for the electron thermal transport and the MMM7.1 is used for the thermal ion transport.

4. Current ramp-up and sustainment

Plasma discharge #142305 discussed above is chosen as a reference for time-dependent simulations to project to non-inductive ramp-up and sustainment in NSTX-U. This discharge was part of an experimental campaign targeting high-performance, higher elongation and higher aspect ratio plasmas, developed specifically in support of NSTX-U and of next-step ST devices in general. Those experiments were extensively discussed by Gerhardt *et al* [47] and the specific case chosen as a basis for our studies is plotted in figure 22 of that article.

The reference discharge provides the profile for the dominant impurity (Carbon), the rotation profile and effective ion charge $Z_{\rm eff}$, as well as qualitative profile peaking of the electron temperature and density and width of the pedestal in H-mode. Time-dependent simulations have been run with TRANSP with the free boundary Isolver [29]. Figure 3 shows the time traces of the external heating waveforms, the line averaged density, the contributions to the non-inductive current, the elongation, internal inductance and safety factor on-axis. Profiles of density, temperature and current during the RF phase (at 0.25 s) and during the NBI phase (at 3.5 s),

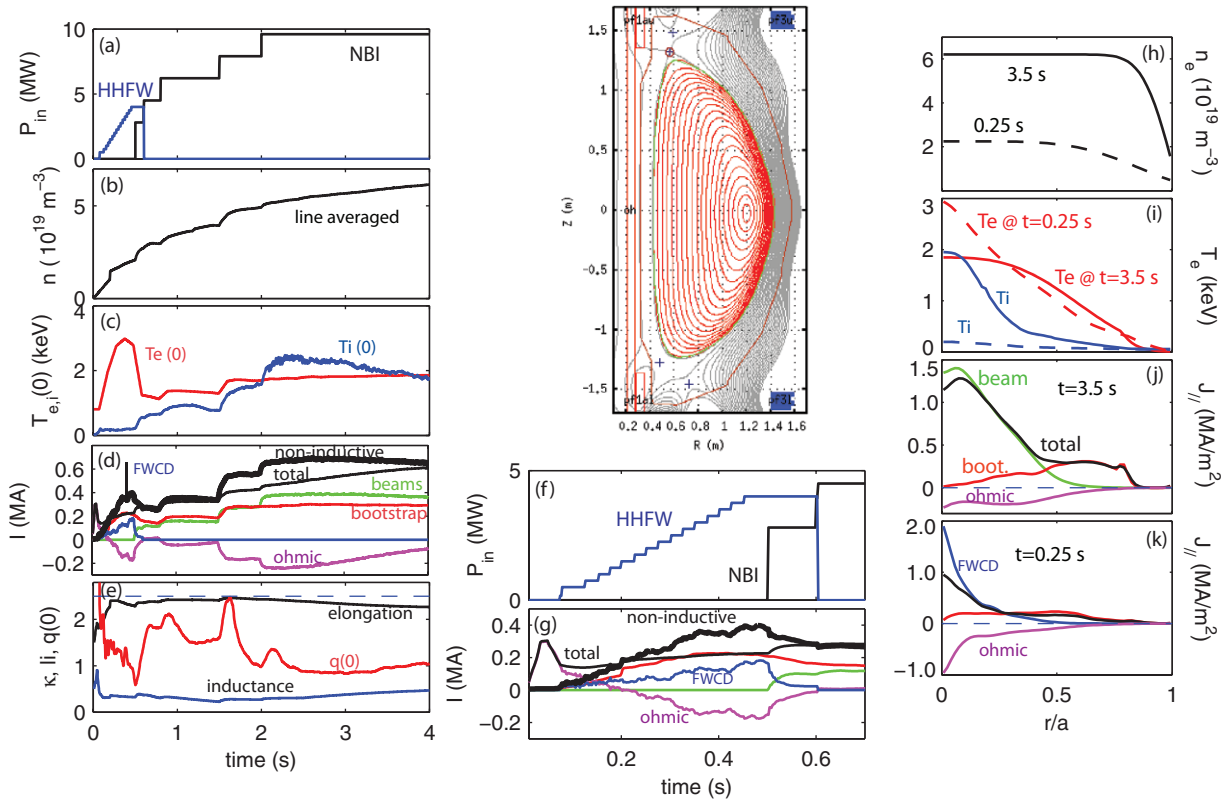

Figure 3. Simulation of a discharge with line-averaged density of $0.75n_G$ that uses up to 4 MW of HHFW and up to 10 MW of NBI to ramp-up and sustain a non-inductive current of 0.7 MA. Left panel: (*a*) injected HHFW and NBI power, (*b*) line averaged electron density, (*c*) central electron and ion temperature, (*d*) total plasma current and individual contributions, (*e*) safety factor on-axis, elongation at the separatrix and internal inductance. Central panel: equilibrium calculated at 3.5 s, (*f*)–(*g*) expanded view of the RF phase. Right panel: profiles of (*h*) density, (*i*) electron and ion temperature at 0.25 s (RF phase) and at 3.5 s (NBI phase), (*j*) current density profiles at 3.5 s, (*k*) current density profiles at 0.25 s.

as well as the free-boundary equilibrium at 3.5 s, are also shown. Up to 4 MW of HHFW power is used starting 50 ms after start-up, continuing until 0.6 s. The HHFW power is turned-off soon after NBI power is turned-on for two reasons: (1) most of the HHFW power is absorbed on the fast ions and (2) the electron absorption of the HHFW drops reducing the fast wave driven current.

Density profiles are prescribed as a function of time and the whole profile is rescaled so that the Greenwald fraction is constant within 10% during H-mode. Since the density profiles are prescribed, but the total current is calculated, this hypothesis is satisfied only as far as the variation in the NBI driven current is small. The simulation shown in figure 3 assumes a density that is 75% of the Greenwald fraction. Future simulations will improve this assumption by using a feedback control over the electron density amplitude [52] to ensure tracking of a particular Greenwald fraction throughout the plasma current ramp-up. The L-H transition is imposed at 150 ms by prescribing a pedestal in the input profiles, of comparable width in the density and temperature profile, as shown in figures 3(*h*) and (*i*) The density profile in H-mode is assumed to be flat. Considering the lower collisionality expected in NSTX-U compared to NSTX, the density profiles assumed in H-mode in these simulations are probably too flat. Future experiments and a systematic validation of particle transport will help to refine these assumptions and improve the projections to higher non-inductive current.

It should be noted that predictive simulations of the NBI-heated flattop phase assume classical fast ion behavior. In reality, fast ions may drive instabilities, which—in turn—enhance fast ion transport. Redistribution of fast ions would result in a broadening of the NB heating profile and, therefore, in a broadening of the electron and ion temperature profiles. In order to reduce the number of assumptions and adjustable parameters in the simulations, those effects are neglected in the present work. Instead, analytic profiles that reproduce the electron temperature profile measured on NSTX are used.

The electron and ion temperature profiles are predicted during the RF phase with the MMM7.1 transport model, which was found to reproduce amplitude and peaking of the experimental electron temperature profile in RF heated discharges. They are predicted also during the NBI phase, when the current is below 400 kA. During the NBI phase and at plasma current above 500 kA, the electron temperature is input as analytic form, while the ion temperature is predicted by the MMM7.1. In practice, the simulation is first run with predictive electron transport from MMM7.1. Then, analytic, broader profiles, are constructed using two constrains:

(*a*) the central temperature is that predicted with the MMM7.1 model and (b) the pedestal width is the same as the pedestal density, at $r/a = 0.85$, and the pedestal height is about 500 eV. The simulation is then run a second time using these electron temperature profiles. The electron and ion temperature profiles are shown in figure 3(*i*). The ion temperature profile outside $r/a = 0.85$ is from NSTX experiments. As shown in figure 2, no pedestal is clearly evident in the ion temperature profile. The peaked electron temperature profile during the RF phase is a consequence of the core heating, the broad electron temperature profile during the NBI phase is from the analytic formulation. The electron temperature profile outside the pedestal top decreases exponentially, which causes a very small current in this region. The large Ohmic contribution during the RF phase is a consequence of the choice of imposing a zero surface voltage and indicates that profiles are far from relaxation. This is also seen in the expanded view of the RF phase in panels (*f*) and (*g*).

Starting from the magnetic equilibrium of the reference discharge, we have first used Isolver standalone to reconstruct a sequence of boundary shapes in NSTX-U geometry consistent with the new poloidal field coil setup. The sequence of boundary shapes satisfies in the flattop an elongation of 2.75, a triangularity of 0.75 and a squareness of 0.1. Isolver would also calculate the coil current required to obtain this shape, although this information is not used at this time. Instead, the plasma boundary is used in TRANSP by Isolver in a χ^2 minimization to calculate an equilibrium solution that minimizes the difference with the input plasma boundary. The χ^2 minimization is the first step required in the predictive calculations, during which coil currents are also calculated. In a second step, the calculated currents are used as an input and the simulation is run again with coil currents and plasma equilibrium evolved self-consistently as a circuit, with additional constraints to limit coil current excursions and with feedback control for the plasma horizontal and vertical position. The outer gap in these simulations is about 12.5 cm and it is maintained fixed during the current ramp-up and sustainment phase, not an optimal value for ensuring broad deposition and optimal current profile control, as discussed by Gerhardt [6].

The plasma current waveform during the first 50 ms reproduces the standard solenoidal operation in NSTX, with a fast ramp-up to 300 kA in 50 ms. In the simulation the Ohmic system cannot be excluded completely and the transition from inductive to non-inductive at 50 ms is imitated by a switch in the boundary conditions of the poloidal field diffusion equation solution, from matching the total current value to matching zero loop voltage. This is done because the goal of this simulation is to understand (a) how fast (or slow) the non-inductive current rises (b) what combination of beams and electron density maintains the target elongation, a central safety factor above one and internal inductance around 0.65. For this reason the total current needs to be calculated and one way of doing this is to enforce the surface voltage. Since at this stage, the choice of the voltage level is arbitrary, the value of zero has been chosen for simplicity and to obtain an estimate of how long it takes to get to a steady-state.

Like any inductive circuit, the plasma will respond to external forcing to avoid changes in the enclosed flux. In this case this is a current in the direction opposite to the non-inductive current, which will reduce the amplitude of the total current. In figure 3(*d*) this is seen as a drop in the Ohmic contribution, which coincides with the increase in the direct fast wave driven current. Eventually the solution will converge to a steady state solution on the time scales of current diffusion, with zero ohmic current and 100% non-inductive current.

The simulation scenario shown in figure 3 achieves 700 kA of non-inductive current in about 2 s, and sustains a confinement level of $H98 \simeq 1$, by using about 10 MW of NBI power. The plasma current is sustained for the duration of the NBI pulse by a combination of NBCD and bootstrap current, with comparable contributions.

The evolution of the internal inductance, of the elongation and of the safety factor on-axis, shown in figure 3(*d*) reveal some of the typical problems encountered in these simulations. First, the second NBI system has high current-drive efficiency, which is good. However, the large beam pressure makes it difficult to maintain the plasma shape during the phase of non-inductive plasma current sustainment. This is indicated in figure 3(*e*) by the slow decay of the elongation starting from 1.5 s and the slow increase in the internal inductance. This is the time when two NBI sources at 80 kV are injected from the second NBI system, with tangency radii of 110 and 120 cm. Injecting these NBI sources any time before 1.5 s results in a lack of convergence in the equilibrium solution and in difficulties in sustaining the desired plasma shape. Injecting sources with lower energy would avoid this problem, but would also sustain a lower non-inductive plasma current. The largest tangency radius NBI source runs at 65 kV from 0.5 s, to help to sustain a broad current profile. Using higher energy sources exacerbates the issues with equilibrium convergence and plasma shape control mentioned above. The small tangency NBI system is used from 0.5 s with all three NBI sources at 80 kV.

Another issue encountered is maintaining the safety factor on-axis above one. It is found that operating with densities above 70% of the Greenwald limit, helps in maintaining $q > 1$ during the phase of sustainment of non-inductive current. The safety factor drops below unity also during the HHFW phase, mainly because of the large core current density. In the simulation in the figure, the rapid rise in the electron density helps maintain values above unity, by reducing the fast wave current drive efficiency. Since Alfvénic activity is important in Spherical tokamaks and can lead to disruptions in the ramp-up phase, future simulations need to combine the evolution of the plasma with stability analysis and advice on plasma trajectories that are MHD stable.

These simulations assume no fast ion diffusion. Calculations in the flattop phase, under different assumptions on the diffusion coefficient, indicate a relaxation of the current profile and larger values of the minimum safety factor [6]. This will be addressed in future simulations, after characterization of the second NBI system and experimental validation using TRANSP.

5. Addressing challenges to non-inductive ramp-up

Non-inductive ramp-up is challenging in both experiments and simulations, for several reasons. Most obviously, one must provide sufficient current to replace the inductive current contribution. Contrary to an inductive discharge, where current diffuses from the outside, in a non-inductive ramp-up the externally driven current profiles are determined by the characteristics of the external sources. On NSTX-U, the HHFW power would produce centrally peaked current and pressure profiles, while the NBI power would provide more flexibility by combining sources with appropriate energy and tangency radii. In simulations, current profiles that are too peaked compromise the equilibrium convergence because of large gradients in space and time. Internal transport barriers develop in the presence of peaked pressure profiles during the HHFW phase, leading to simulations that are unstable against ballooning instabilities and that evolve into a disruption. A challenge is therefore finding a combination of heating and current drive sources that, in addition to satisfying the requirement of high current drive efficiency and accessibility at low density and low temperature, also sustains MHD stable profiles. This section shows that NBI is not effective at driving current in a low density, low temperature target, that HHFW can instead be used more effectively in the start-up and that EC heating improves HHFW absorption and current drive efficiency of the HHFW. In the absence of a validated thermal transport model in these plasma regimes and of similar experiments on other devices to be used as a reference, the purpose of these simulations is not to provide solutions, but rather to address challenges and issues, as well as provide guidance for experimental validation. All simulations discussed in this and in the next section use a waveform for the plasma current, which has a fast ramp to 300 kA in 50 ms and then a slower ramp to 900 kA in 2.5 s. The simulations use the total current as a boundary condition, thus the ohmic current profile will be determined by the difference between the target current and all the non-inductive contributions: bootstrap and externally driven current. The goal of the simulations is to maximize the non-inductive current after start-up at levels close to the requested current.

5.1. Using neutral beams at start-up

In typical NSTX discharges neutral beams are injected into the ohmic plasma at currents not less than 300 kA, to ensure confinement of the fast ions and maintain the shine-thru below 50% of the injected power, as well as to limit impurity accumulation. Figure 4 shows a simulation of the early ramp-up phase in NSTX-U geometry, with maximum nominal toroidal field of 1 T.

In this simulation the three neutral beam sources at low-tangency radius (first beamline) are injected from 25 ms, and one source at higher tangency radius after 50 ms, in this sequence: 65 kV and 70 cm at 25 ms, 70 kV and 60 cm at 35 ms, 75 kV and 50 cm at 50 ms, 65 kV and 130 cm at 200 ms. Different combinations of sources in the first beamline result in variations in the driven current during the first 100 ms that are within 10% of the values shown. Instead, different combinations of sources from the second beam line with higher energy and/or tangency radius of 110 cm and 120 cm result in large beam pressure and problems in the equilibrium calculations. In order to run more self-consistent simulations in this phase, the thermal transport, the beam heating, the beam current and the fast-ion distribution have to be assessed. As seen in the figure, most of the power injected during the first 100 ms of discharge is lost via shine-through, with orbit losses representing a constant contribution.

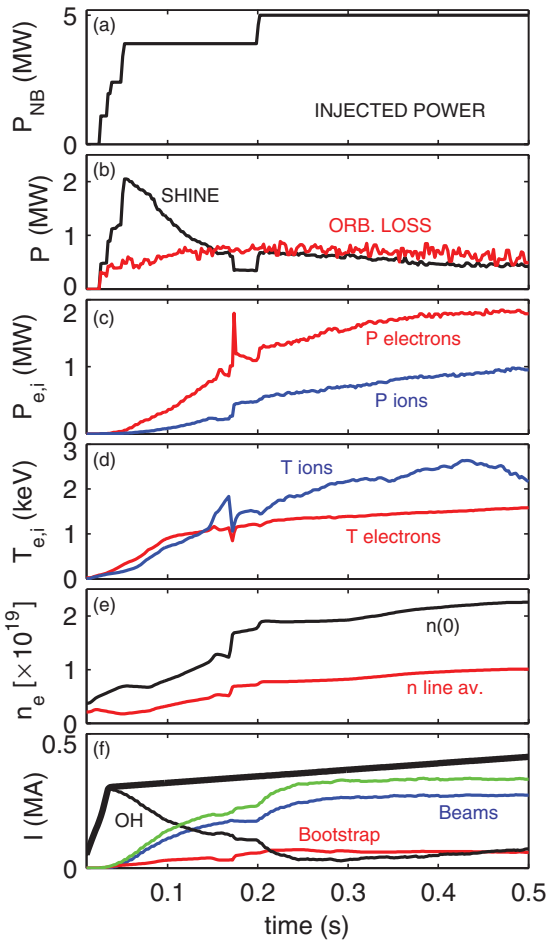

Figure 4. Simulations of NSTX-U at $B_T = 1$ T. (*a*) NBI power waveform, (*b*) shine-thru and orbit loss power, (*c*) power absorbed on the electrons and on the ions, (*d*) central electron and ion temperature, (*e*) central and line averaged density, (*f*) plasma current waveform (black, thick) and contributions to the total current.

The level of current driven before 200 ms can probably be optimized with an adequate combination of the beam energy, tangency radius, and using beam modulation, all options that will be addressed in dedicated experiments on NSTX-U. However, it appears from figure 4 that the first 50 ms of the discharge needs an additional source of current that cannot be provided by the NBI only.

5.2. Driving current with HHFW at start-up

In contrast to the NBI, HHFW power is effective at heating the plasma at low density, both in the electron and the ion channel, depending on the phasing of the antenna [37].

The HHFW system can potentially couple more than 4 MW, stepped-up at a rate of 1 MW every ms. In practice, a significant fraction of the power can be lost to the scrape-off layer and deposited on the divertor, flowing along the magnetic field lines, rather than in the core plasma [36, 53]. The edge density and the location of the fast wave cut-off play an important role in the edge loss mechanisms [54]. These experimental conditions cannot be modeled with the tools available to us in time-dependent simulations. There is no model for the scrape-off-layer plasma in front of the antenna in TORIC, and all the input power is assumed to be absorbed. Losses are therefore taken into account by rescaling the input power to the simulation.

Figure 5 compares two cases that differ in the power step-up rate. In one case 4 MW are ramped-up in 100 ms, while in the second case they are ramped in 200 ms. These assumptions are equivalent to assuming that—for 6 MW injected with a square waveform—only a fraction is absorbed in the plasma, which gradually increases from 10% to 65%. Stated differently, losses reduce from 90% at 20 ms down to 30% after 100 or 200 ms. The assumption that most of the power is lost at the earliest times is consistent with previous experiments on NSTX, where it proved to be difficult to couple the HHFW power into a CHI plasma target. On the other hand, assuming that the minimum level of losses is about 30% at 100 ms is probably optimistic in light of those experiments. However, it is expected that at the higher toroidal magnetic field in NSTX-U and with the recent upgrade to the HHFW antenna, the scrape-off-layer losses will be significantly reduced [54]. Figure 5 should therefore be interpreted as an indication of an upper limit to the fraction of allowable power loss in order to drive the current that is needed to ramp the current non-inductively.

The phasing of the antenna used here corresponds to a parallel wavenumber of 8 m^{-1}, the setting usually adopted in NSTX experiments. Simulations done using the three values of antenna phasing indicate that this intermediate wavenumber is the most favorable for driving current in the start-up plasma.

As shown in figure 5, the driven current has a maximum in the first 200 ms of discharge, then it drops. Increasing density decreases current drive efficiency, which is proportional to temperature and inversely proportional to density [55]. After 300 ms of discharge, the electron absorption also decreases, contributing to the drop in the calculated direct driven current.

With reference to the previous section, the NBI is more effective in H-mode, where the higher density reduces shine-thru and losses, while the HHFW is more effective at driving current in L-mode and in the early H-mode phase, where the density is lower. Ramp-up should combine both sources and use HHFW to prepare a target plasma where NBI can be used with minimum losses. These simulations have q profile with reverse shear in the core until about 120 ms, when the FWCD is maximum, then the safety factor profile evolves monotonically and sustains a minimum above unity.

One of the challenges that need to be addressed in experiments is providing good coupling of the HHFW to the low density, low temperature start-up plasma. One of the challenges to be addressed in the simulations is to imitate experimental-like

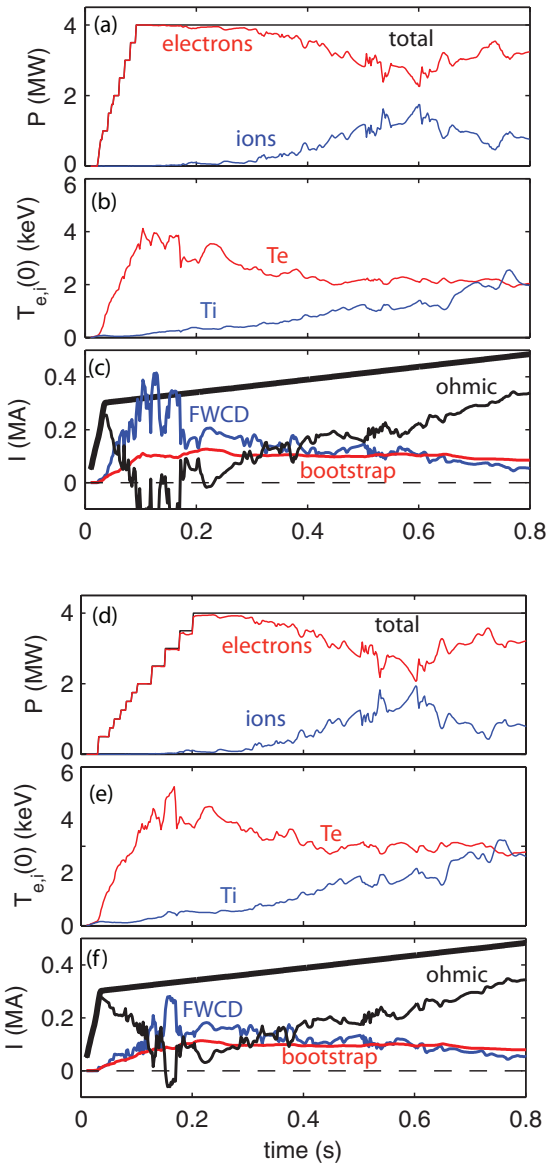

Figure 5. Comparison between two simulation discharges with 4 MW of HHFW power and different power ramp-up rate. ((*a*), (*d*)) Injected power (black) and power absorbed on the electrons (red) and on the ions (blue). ((*b*), (*e*)) central value of electron (red) and ion (blue) temperature. ((*c*), (*f*)) total requested current (thick), bootstrap (red), FW (blue) ohmic (black) current contribution.

conditions, and allow variations in the outer gap of the plasma. As discussed previously, the radial position of the plasma is controlled in these simulations.

6. Preparing a target plasma with ECH

EC waves are a very effective mean for heating the NSTX-U start-up plasma to high temperature in a short time, because of the good accessibility at low density. Figure 6 shows time-dependent simulations where the 1 MW of EC power is applied to the start-up plasma. The target plasma (current, magnetic field) is the same used in the simulations discussed in the previous sections. The initial density and temperature profiles before 10 ms are taken from CHI experiments with

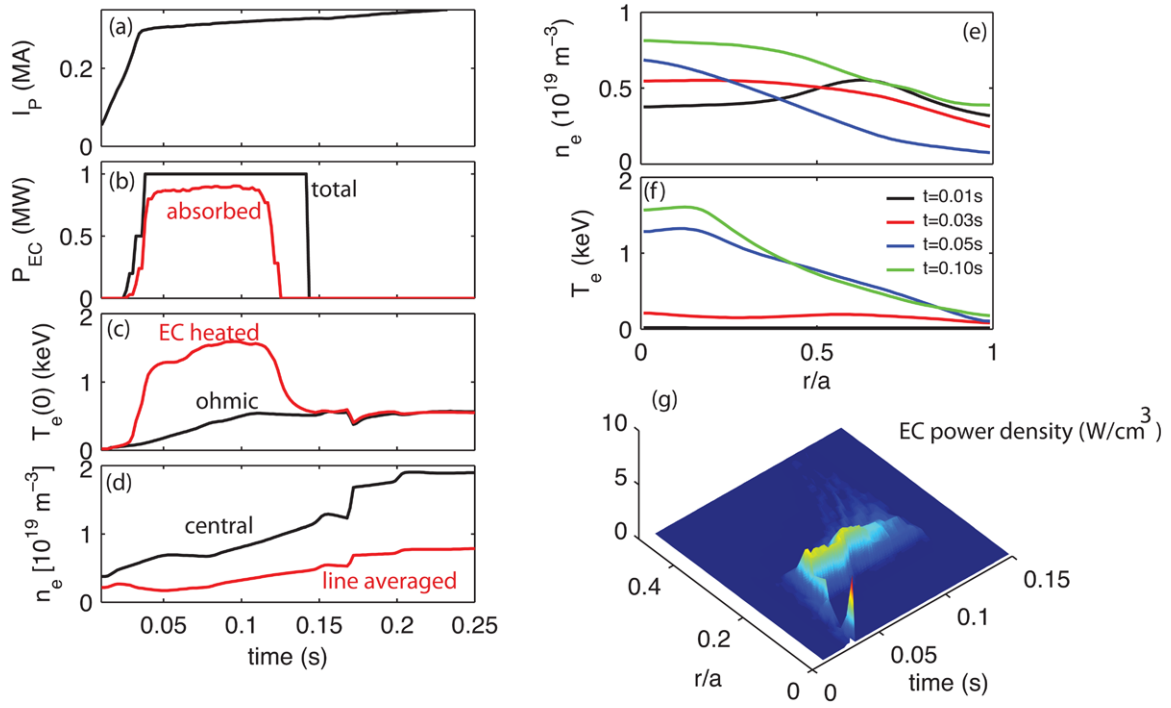

Figure 6. Simulation of EC heating. Left panel: time traces of (*a*) plasma current, (*b*) injected and absorbed power, (*c*) electron temperature on axis compared with an ohmic plasma, (*d*) central and line-averaged density. Right panel: profiles of (*e*) electron density (*f*) electron temperature and (*g*) EC heating profile.

solenoidal assist [24]. The CHI target plasma has typically a very hollow temperature profile, which is peaked off-axis at about $r/a = 0.7$ and that has a central value of about 10 eV. The density profile is also hollow at 10 ms and quickly broadens and flattens, with central value of about 0.5×10^{19} m^{-3}, as shown in figures 6(*e*) and (*f*) respectively. In the case illustrated here, where a CHI plasma is coupled to solenoidal current, the evolution of the plasma parameters after 10–15 ms is in practice the same as that of a standard inductive discharge.

The initial electron temperature profile is evolved in time using the MMM7.1 transport model. Simulations with other transport models result in differences in the predicted temperature within 10% and are not shown here.

In the simulations shown in figure 6 the EC heating is turned-on at 20 ms and the power stepped up to 1 MW within the first 35 ms of discharge. The absorption, initially very low, increases to 20% when the central temperature exceeds 400 eV and to 75% when the temperature exceeds 1 keV. Only first pass absorption is accounted for in these simulations. The flattening in the temperature profile for $r/a < 0.2$ is a consequence of the highly localized heating profile, as shown in figure 6(*g*). For a more detailed analysis of first pass absorption for the O-mode injection in NSTX-U the reader is referred to the work by Taylor *et al* [41].

Figure 6(*c*) shows a comparison with the simulation of an ohmic discharge, which uses the same density profiles, but no EC heating. Compared to the ohmic discharge, the EC waves are very effective at heating the plasma from a few tens of eV to about 1 keV in less than 30 ms. However, the plasma becomes overdense to the EC waves with increasing density, reducing the time window where the EC heating can be applied to the first 100–150 ms of the discharge. The optimal density rise must be assessed in experiments and it will be a compromise between a desire for optimized EC heating and the need for avoiding impurity accumulation. Since one of the goals of NSTX-U is to demonstrate non-inductive startup, future simulations need to address the coupling of EC waves to a CHI plasma with no solenoidal assist.

6.1. Improving HHFW access with ECH

EC waves heat the plasma very effectively to prepare a target where HHFW can be absorbed more favorably. Figure 7 compares two simulations with the same HHFW configuration, one with and one without EC. It is found that the fast wave direct current increases by about 10% when the HHFW, using antenna phasing that corresponds to $k_\parallel = 8$ m^{-1}, is combined with the EC. However, a significant improvement with respect to not using the EC occurs when the lowest antenna phasing that corresponds to $k_\parallel = 3$ m^{-1} is used, as shown in figure 7. Up to 3 MW of HHFW power are coupled in the start-up plasma, at a rate that corresponds to assuming between 60% and 75% losses during the EC heated phase. After the EC phase the HHFW power is stepped-up from 2 MW to 3 MW, equivalent to assuming that the losses reduce from 60% to 50%. The parallel wave vector used here, $k_\parallel = 3$ m^{-1}, favors absorption on the thermal ions, as is shown in the left panel of figure 7. In the case without EC the electron temperature remains in the range of 500 eV, there is almost no direct fast wave current and all the non-inductive current is driven by the bootstrap current.

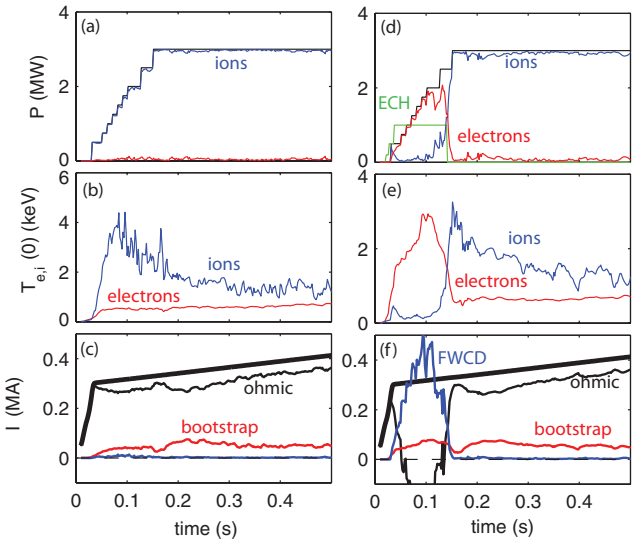

Figure 7. Comparison between two simulations without (left) and with EC heating (right) for parallel wavenumber of $k_{\|} = 3\ \mathrm{m}^{-1}$. (*a*) Injected power and power absorbed by the ions and the electrons. (*b*) central value of electron and ion temperature (*c*) total current waveform and contributions: ohmic (black), FWCD (blue), bootstrap (red).

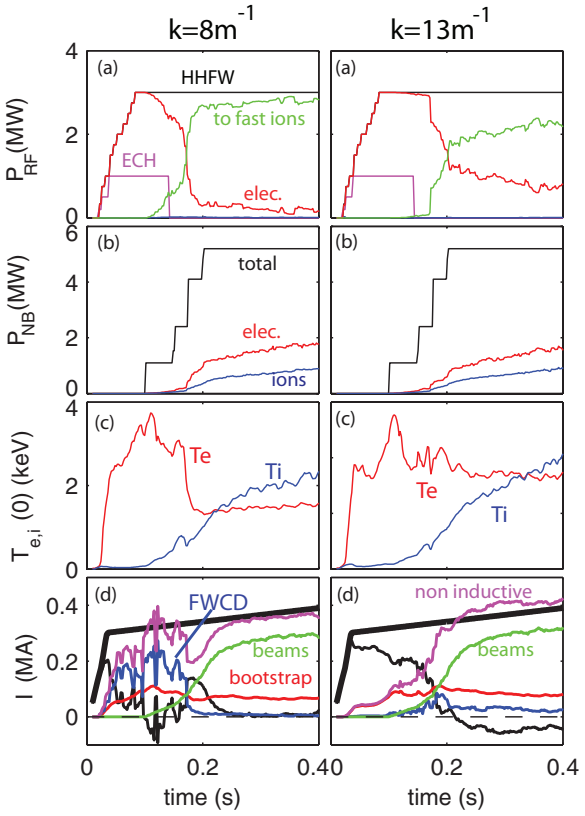

Figure 8. Simulations with EC, HHFW and NBI at start-up for $k_{\|} = 8\ \mathrm{m}^{-1}$ (left) and for $k_{\|} = 13\ \mathrm{m}^{-1}$ (right). (*a*) EC waveform (magenta), HHFW injected power and power absorbed to the electrons (red), to the ions (blue) and to the fast ions (green). (*b*) Neutral Beam injected (black) power, and absorbed by the electrons (red) and by the ions (blue). (*c*) Central value of electron and ion temperature. (*d*) current waveform (thick black) and contributions: FWCD (blue), beam current (green), ohmic (black) and bootstrap (red), the total non-inductive current is also shown for comparison (magenta).

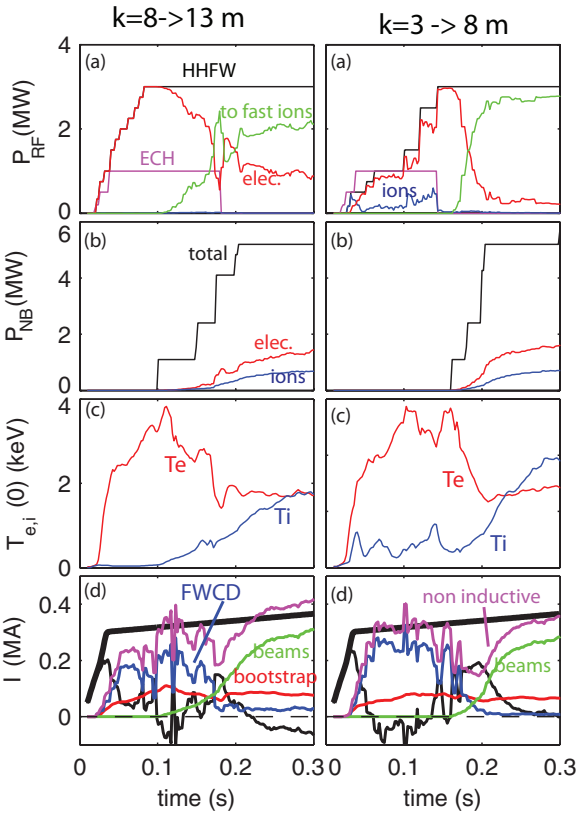

Figure 9. Simulations with EC, HHFW and NBI at start-up for a dynamic change of phasing in the antenna: transition from $k_{\|} = 8\ \mathrm{m}^{-1}$ to $k_{\|} = 13\ \mathrm{m}^{-1}$ at $t = 0.18$ s (left) and from $k_{\|} = 3\ \mathrm{m}^{-1}$ to $k_{\|} = 8\ \mathrm{m}^{-1}$ at 0.14 s (right). (*a*) EC waveform (magenta), HHFW injected power and power absorbed to the electrons (red), to the ions (blue) and to the fast ions (green). (*b*) Neutral Beam injected (black) power, and absorbed by the electrons (red) and by the ions (blue). (*c*) Central value of electron and ion temperature. (*d*) current waveform (thick black) and contributions: FWCD (blue), beam current (green), ohmic (black) and bootstrap (red), the total non-inductive current is also shown for comparison (magenta).

When the plasma is pre-heated with 1 MW of EC power, the electron temperature increases rapidly to 1 keV, as discussed in the previous section. Although the $k_{\|} = 3\ \mathrm{m}^{-1}$ antenna phasing favors ion absorption, a significant fraction of the power is predicted by TORIC to be absorbed on the electrons because of the large electron temperature. This results in a significant increase in the driven current during the EC phase. As little as 1–2 MW of absorbed HHFW power are sufficient to drive 300 kA non-inductively, a significant improvement over using HHFW alone.

Ideally, a fully non-inductive start-up and ramp-up should use all three sources to maximize benefits: the EC to pre-heat the CHI start-up plasma and prepare a target plasma, the HHFW to maximize the non-inductive current at low density and then the NBI to ramp the current after the L-H transition, when the current drive efficiency of the HHFW is reduced. Figure 8 shows the plasma evolution for the other two values of phasing, with $k_{\|} = 8\ \mathrm{m}^{-1}$ and $k_{\|} = 13\ \mathrm{m}^{-1}$. A comparison between figures 7 and 8 indicates that an ideal situation would be to dynamically change the antenna phasing, using first the lowest $k_{\|}$, to take advantage of the synergy with the EC waves,

then the higher $k_{\|}$ to reduce absorption on the fast ions and maximize the absorption on the electron. Figure 9 imitates this situation by comparing a case where $k_{\|}$ is increased from 8 m^{-1} to 13 m^{-1} and a case where $k_{\|}$ is increased from 3 m^{-1} to 8 m^{-1}. The maximum power in H-mode is the same in the two cases, but there is a significant difference in the input power during the first 100 ms of discharge. When the HHFW starts with the lowest available $k_{\|}$, the current drive efficiency is about twice as large and only 1 MW of power needs to be absorbed in the core plasma to drive about 300 kA of FWCD at start-up. However, these benefits cease as soon as the EC phase is over and at least 4 MW of absorbed power are needed later on to sustain the same current. As discussed in the previous section, the absorption on fast ions is an issue. However, the NB current drive increases rapidly after 200 ms, indicating that a transition between the HHFW and NBI is appropriate at this time. The current drive efficiency of the HHFW is anyway too low in this phase to contribute to the non-inductive current ramp-up.

7. Conclusions

Non-solenoidal plasma formation and sustainment presents scientific and operational challenges. First, there is the demonstration of non-inductive sustainment of plasmas that are MHD stable and that sustain an adequate confinement level and optimal performance. This should be demonstrated at incrementally higher values of plasma current. Second, the non-inductive sustainment needs to be extended back in time and to lower current, and possibly combined with control of the density evolution, of the kinetic and current profiles and of the plasma pressure to magnetic field pressure ratio. The phase right after start-up is particularly challenging. The externally driven current must replace the solenoidal current, by avoiding excessive core peaking of the current profiles. Radio-Frequency waves, like EC and HHFW, have good accessibility at low density and are effective at heating the low temperature start-up plasma. However, good absorption of the HHFW power must be ensured in start-up conditions, as well as adequate control of the plasma position across the L-H transition, to avoid back transitions and RF power loss, due to large changes in the gap between the antenna and the last closed flux surface.

EC waves might be the only effective way of optimizing current drive at start-up. By heating the plasma in the electron channel, the EC heating prepares a background plasma where HHFW power can effectively drive current. An interesting synergy is observed in the simulations between the EC and HHFW. Depending on the phasing, the fast wave current drive efficiency is maximized and the minimum HHFW power required is reduced. With 1 MW of EC heating, as planned on NSTX-U, as little of 1 MW of HHFW would be needed to drive 300 kA of plasma current.

Independently of the method used to start-up the plasma, either solenoidal, with CHI, or with EC/EBW, the path to fully non-inductive ramp-up on NSTX-U should include all three sources: the EC to pre-heat the CHI start-up plasma, the HHFW to maximize non-inductive current at low density and NBI to ramp-up the current after the L-H transition, when the current drive efficiency of the HHFW is reduced.

Simulations are inherently affected by limits in the models that are used for the predictions. In particular, large uncertainties in the start-up phase come from the lack of validated models for thermal and particle transport that can be applied in this phase. Future simulations will take advantage of improved algorithms for feedback control of plasma density, shape and current.

Acknowledgments

M. Podestà is kindly acknowledged for valuable discussion, S.M. Kaye and J.R. Wilson for carefully reading the manuscript. This work was supported by the U.S. Department of Energy under contract DE-AC02-CH0911466. The digital data for this paper can be found in http://arks.princeton.edu/ark:/88435/dsp011v53k0334

References

[1] Peng Y.-K.M. and Strickler D.J. 1986 *Nucl.Fusion* **26** 769
[2] Peng Y.-K.M., Galambos J.D. and Shipe P.C. 1992 *Fusion Sci. Technol.* **21** 1729
[3] Peng Y.-K.M. *et al* 2005 *Plasma Phys. Control. Fusion* **47** B263
[4] Peng Y.-K.M. *et al* 2009 *Fusion Sci. Technol.* **56** 957
[5] Menard J.E. *et al* 2012 *Nucl. Fusion* **52** 083015
[6] Gerhardt S.P. *et al* 2012 *Nucl. Fusion* **52** 083020
[7] Sabbagh S. *et al* 2006 *Nucl. Fusion* **46** 635
[8] Jobes F. *et al* 1984 *Phys. Rev. Lett.* **52** 1005
[9] Shiraiwa S. *et al* 2004 *Phys. Rev. Lett.* **92** 035001
[10] Shinya T. *et al* 2015 *Nucl. Fusion* **55** 073003
[11] Preinhaelter J. and Kopecky V.J. 1973 *Plasma Phys.* **10** 1
[12] Mjølhus E. 1984 *J. Plasma Phys.* **31** 7
[13] Hansen R. *et al* 1988 *J. Plasma Phys.* **39** 319
[14] Forest C.B. *et al* 1992 *Phys. Rev. Lett.* **68** 3559
[15] Sykes A. 2005 Plasma current formation in MAST without use of central solenoid *32nd EPS Conf. on Plasma Physics (Tarragona, 27 June–1 July 2005)* vol 29C P-4.112 http://epsppd.epfl.ch/Tarragona/pdf/p4_112.pdf
[16] Shevchenko V. *et al* 2010 *Nucl. Fusion* **50** 022004
[17] Jackson G.L. *et al* 2011 *Nucl. Fusion* **51** 083015
[18] Uchida M. *et al* 2012 *Proc. 24th. Int. Conf. on Fusion Energy (San Diego, USA, 8–13 October 2012)* www-naweb.iaea.org/napc/physics/FEC/FEC2012/papers/333_EXP618.pdf
[19] Shevchenko V. *et al* 2015 Long pulse EBW start-up experiments in MAST *EPJ Web Conf.* **87** 02007
[20] Inomoto M. *et al* 2015 *Nucl. Fusion* **55** 033013
[21] Jarboe T.R. 1989 *Fusion Technol.* **15** 7
[22] Raman R. *et al* 2010 *Phys. Rev. Lett.* **104** 095003
[23] Nelson B.A. *et al* 2011 *Nucl. Fusion* **51** 063008
[24] Raman R. *et al* 2013 *Nucl. Fusion* **53** 073017
[25] Raman R. *et al* 2014 *IEEE Trans. Plasma Sci.* **42** 2154
[26] Kaye S.M. *et al* 1999 *Fusion Technol.* **36** 16
[27] Ono M. *et al* 2000 *Nucl. Fusion* **40** 557
[28] Hawryluk R.J. 1980 An empirical approach to tokamak transport *Physics Close to Thermonuclear Conditions* vol 1 ed B. Coppi *et al* (Brussels: Commission of the European Communities) p 19
[29] Andre R. 2012 TRANSP/PTRANSP Isolver free boundary equilibrium solver *Bull. Am. Phys. Soc.* **57** 12

[30] Jardin S.C., Pomphrey N. and Delucia J. 1986 *J. Comput. Phys.* **66** 481
[31] Jardin S.C., Bell M.G. and Pomphrey N. 1993 *Nucl. Fusion* **33** 371
[32] Goldston R.J. *et al* 1981 *J. Comput. Phys.* **43** 61
[33] Pankin A. *et al* 2004 *Comput. Phys. Commun.* **159** 157
[34] Honda M., Kikuchi M. and Azumi M. 2012 *Nucl. Fusion* **52** 023021
[35] Ono M. *et al* 2001 *Nucl. Fusion* **41** 1435
[36] Hosea J. *et al* 2008 *Phys. Plasmas* **15** 056104
[37] Bertelli N. *et al* 2014 *AIP Conf. Proc.* **1580** 310
[38] Brambilla M. 2002 *Plasma Phys. Control. Fusion* **44** 2423
[39] Ehst D.A. and Karney C.F.F. 1991 *Nucl. Fusion* **31** 1933
[40] Taylor G., Ellis R.A., Harvey R.W., Hosea J.C and Smirnov A.P 2012 *EPJ Web Conf.* **32** 02014
[41] Taylor G. *et al* 2015 *EPJ Web Conf.* **87** 02013
[42] Harvey R.W. and McCoy M.G. 1993 *Proc. of the IAEA Technical Committee on Advances in Simulation and Modeling of Thermonuclear Plasmas* (Vienna: IAEA) p 489
[43] Smirnov A.P. *et al* 2009 *Proc. of the 15th Workshop on ECE and ECRH* (Singapore: World Scientific) p 301
[44] Lin-Liu Y.R., Chan V.S. and Prater R. 2008 *Phys. Plasmas* **6** 3934
[45] Marushchenko N.B. *et al* 2011 *Phys. Plasmas* **18** 032501
[46] Taylor G. *et al* 2012 *Phys. Plasmas* **19** 042501
[47] Gerhardt S.P. *et al* 2011 *Nucl. Fusion* **51** 073031
[48] Rafiq T. *et al* 2013 *Phys. Plasmas* **20** 032506
[49] Tang W.M. 1986 *Nucl. Fusion* **26** 1605
[50] Honda M. and Fukuyama A. 2006 *Nucl. Fusion* **46** 580
[51] Houlberg W.A. *et al* 1997 *Phys. Plasmas* **4** 3230
[52] Boyer M. *et al* 2015 *Nucl. Fusion* **55** 053033
[53] Perkins R.J. *et al* 2012 *Phys. Rev. Lett.* **109** 045001
[54] Bertelli N. *et al* 2014 *Nucl. Fusion* **54** 083004
[55] Fisch N.J. 1987 *Rev. Mod. Phys.* **59** 175